Carbon induced metal dusting of iron-nickel-chromium alloy surfaces

Palasantzas, G; DeHosson, JTM

Published in:
Applied Surface Science

DOI:
10.1016/j.apsusc.2004.01.061

Publication date:
2004

Available online at www.sciencedirect.com
SCIENCE DIRECT®
Applied Surface Science 229 (2004) 190–196
applied surface science
www.elsevier.com/locate/apsusc

Carbon induced metal dusting of iron–nickel–chromium alloy surfaces: a scanning auger microscopy study

G. Palasantzas*, H.J. Kooij, J.Th.M. DeHosson

Department of Applied Physics, Materials Science Centre and Netherlands Institute for Metals Research, University of Groningen, Nijenborgh 4, 9747 AG Groningen, The Netherlands

Received 18 November 2003; received in revised form 28 January 2004; accepted 28 January 2004

Available online 5 March 2004

Abstract

In this work, we present an investigation on metal dusting of iron–nickel–chromium (Fe–Ni–Cr) alloy surfaces using scanning auger microscopy. It is shown that the formation of surface Cr-oxide and the surface finish condition can strongly influence and interrupt this catastrophic phenomenon. The accumulation of C within the metal matrix was not always prevented by the Cr-oxide layer. The formation of Cr-oxide was accompanied by a depleted Cr layer (next to the oxide layer) with a depth of several hundreds of nanometers. The depleted Cr layer was significantly broader if the C diffusion within the metal matrix was prevented, while no preferential enrichment of Ni or Fe close to the alloy surface was observed.

PACS: 81.65.K; 81.65.M; 61.16.Ms; 61.16.-d

Keywords: Corrosion; Oxidation; Auger electron microscopy; Electron microscopy

1. Introduction

In general, exposure of metal and alloy surfaces to carbonaceous gases can lead to carburization and metal dusting [1–20]. Carburization is an internal carbide formation, occurring at high temperatures and low carbon activities $A_C < 1$, which leads to embrittlement, cracking and loss of oxidation resistance [1–10]. Metal dusting is a disintegration of metals to a dust of carbon (C) and metal particles, occurring in syngas ($CO - H_2$) and hydrocarbons at C activities $A_C < 1$ and at 400–800 °C [10–20].

Different dusting mechanisms have been observed for nickel (Ni) and iron (Fe) based alloys [12,15,21–24]: (i) In Ni-base alloys there is a direct inward or internal growth of graphite where no unstable carbide is formed as an intermediate reaction product. Carbon atoms from an oversaturated solution attach to the graphite basal planes, which grow into the metal matrix. (ii) In Fe (and steels) the instable carbide M_3C ($M = Fe, Ni$) (cementite) is formed, which after graphite nucleation decomposes ($M_3C \rightarrow 2M + C$) by inward growth of graphite. The cementite layer is a diffusion barrier for further C ingress increasing A_C, while nucleation of graphite on the surface causes decrease of $A_C \rightarrow 1$. The metal atoms migrate through the graphite and agglomerate to form metal nanoparticles (~20 mm), which further catalyze C deposition

* Corresponding author. Tel.: +31-5036-34272; fax: +31-5036-34881.
E-mail address: g.palasantzas@phys.rug.nl (G. Palasantzas).

0169-4332/$ – see front matter © 2004 Elsevier B.V. All rights reserved.
doi:10.1016/j.apsusc.2004.01.061

from the gas phase (i.e., often growth of C-filaments from the metal particles).

Metal dusting can be inhibited by the presence of sulfur (S) [16,25,26]. The C transfer is retarded by adsorbed S, which also suppresses the nucleation of graphite and thus interrupts metal dusting of Fe-based alloys. In the critical temperature range where metal dusting occurs, the S addition needed to suppress the C attack is rather low, i.e., $H_2S/H_2 \approx 10^{-7}$ at 500 °C [27]. Although currently the only way to protect materials against metal dusting is the addition of S-containing compounds, S often deactivates catalysts needed in various processes. Besides S, another important way to prevent metal dusting is the formation of protective oxide layers, which are Cr-rich oxide layers [27]. This Cr-oxide layer can be formed on ferritic steels with >11%Cr, and in austenitic steels with >17%Cr even at low pO_2 as established by the H_2O and CO_2 present in the process gases [27]. Nevertheless, metal dusting may start from defects, which leads to the well-known appearance of pits and holes in high alloy steels. Such defects can be heterogeneities in the surface, inclusions and precipitates (e.g., TiN, WC, NbC), scratches or edges [28]. Defects may also arise from oxide cracking and spalling [27].

The complex processes in the metal dusting of Fe and steels, however, are not fully understood and further studies are necessary. The focus in this work is to examine the influence of Cr-oxide on metal dusting of Ni–Fe alloy systems in relation also to surface finish treatment. This study is performed with scanning auger/electron microscopy (SAM/SEM) with nanometer resolution.

2. Experimental

The apparatus, described in detail elsewhere [29], consists of a UHV (base pressure $\sim 4 \times 10^{-8}$ Pa during Auger analysis) scanning Auger/electron microscope (field emission JEOL JAMP7800F). Under typical imaging conditions which correspond to the accelerating voltage of 10 keV, and electron beam current of $I = 2.4$ nA; the attainable electron beam spot size is ~15 nm. The samples used in the present study were prepared and supplied by TNO (Netherlands Organization for Applied Scientific Research) [1]. Metal dusting took place at a temperature of 600 °C within an atmosphere of 73 vol.% H_2, 25 vol.% CO, and 2 vol.% H_2O [1]. The chemical composition of the samples was 46 wt.% Fe (Fe-based alloy), 20 wt.% Cr, 32 wt.% Ni, 0.7 wt.% Mn, and small amounts of Al, C, and Si.

Auger depth profile analysis was performed by Ar^+ (of energy 3 kV) sputtering at a low rate 0.18 nm/s calibrated with respect to native SiO_2, and AES data were acquired with 400 ms dwell time (acquisition time/eV). For the SAM images the ratio $(P - B)/B$ was recorded with P the intensity at the corresponding element peak-energy for the direct spectrum, and B the background level at the right end of the peak. Such ratio minimizes significantly any topology effects arising from the virtual tilt of the sample surface and its roughness.

3. Results and discussion

Fig. 1 shows the surface topology of the ground (G) sample prepared with SiC#600, and the electropolished (EP) sample. Atomic force microscopy (AFM) indicates that the surface has a rather ordered surface structure (only as topography) with a low rms roughness amplitude ≈3 nm (for scan size >1 μm). On the G + EP prepared surface, there is a thin oxide layer due to oxidation in air, which extends up to a depth of ~5 nm (comparable with the rms roughness amplitude). The sample is homogeneous and consists mainly of Fe, Ni, and Cr as far as AES can resolve. As the depth profile indicates, the Fe and Cr intensity (peak-to-peak: p–p) increases indicating surface oxidation due to both Fe and Cr, while the presence of C is due to typical environmental contamination (hydrocarbons). Similar was the situation for other unexposed samples independent of surface treatment prior to exposure to metal dusting environment.

Besides the as prepared G + EP surface, also the G-surface area is subject to metal dusting environment. Fig. 2a shows the SEM image of the G-surface after undergoing metal dusting processing. The depth profile shows that a Cr-oxide (most likely the stable form Cr_2O_3) layer of thickness ~300 nm is formed, and serves as a protection on the surface against metal dusting. Although the Fe and Ni below the Cr-oxide layer can react with C, the presence of the Cr-oxide prevents any carbide formation and C accumulation

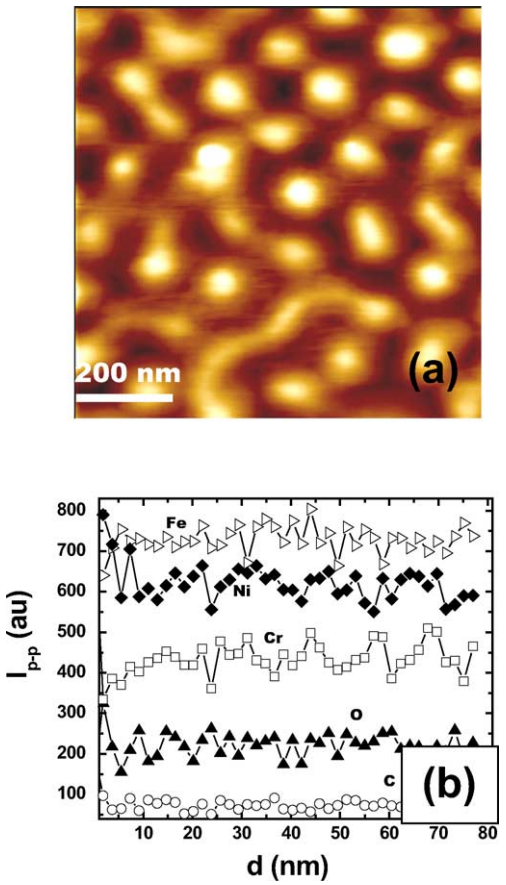

Fig. 1. (a) AFM topography image (scan size 800 nm) of the unexposed ground and electropolished sample surface. (b) Depth profile analysis of the as prepared sample with electron beam size 20 μm.

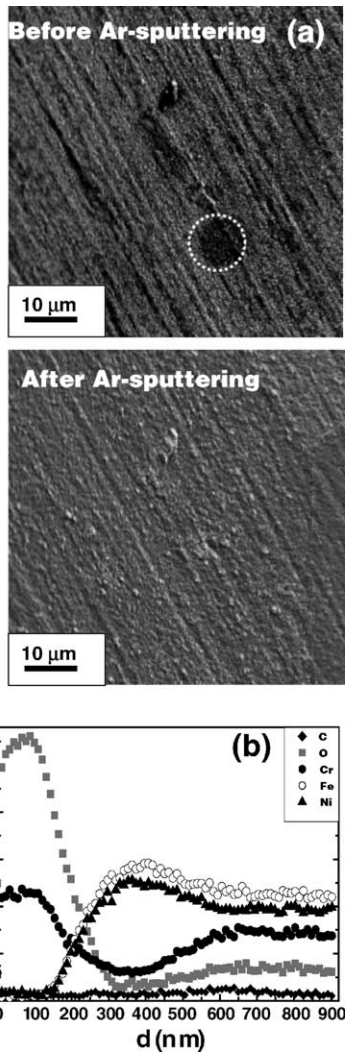

Fig. 2. (a) SEM image of the exposed ground surface: Top as exposed (dotted circle indicates e-beam induced C polymerization during AES data acquisition), bottom after Ar-sputtering. (b) Depth profile analysis of the ground sample with electron beam size 20 μm.

within the metal matrix. Beneath the Cr-oxide layer, there is depletion of Cr, which extends over a depth of ≈400 nm. Deeper within the metal matrix Cr and O recover in composition without any further variation also of Fe being the most possible oxidizing element. Although the G-surface is rougher than the G + EP surface, it appears rather resistant to any metal dusting process indicating that the surface treatment might have blocked C fast diffusion paths towards the metal matrix.

In general, the ability of surface oxide films to inhibit metal dusting depends on the process environment and its influence on the stability of the oxide scale and self-repair after damage [30]. Cr diffusion rates are higher in ferrite than in austenitic and thus protective layers are more likely to be self-repaired at relatively low temperatures in high Cr ferritic steels than in the austenitic steels [27]. Moreover, surface deformation, i.e., by cold working, also favours the formation of a protective layer because the high density of dislocations in cold worked regions may provide easy diffusion paths for Cr to the surface (depending also on the dislocation character). In high Ni-base alloys there is resistant to metal dusting

because of the slower diffusion of C in a Ni-base austenitic matrix. However, it has also been pointed out that the same mechanism will also inhibit the healing of ruptured surface films by retarding the diffusion of Cr at relatively high Ni contents [31].

On the basis of thermodynamics it was believed that increasing Ni content will inhibit metal dusting because of its effect in retarding the formation of the 'intermediate' meta- or unstable carbide M_3C (where M = Fe, Ni) which is fundamental to the mechanism proposed by Grabke et al. [10–20]. As Fig. 2b shows for the G-surface, both the Fe and the Ni increase within the area where Cr is depleted indicating that neither Ni nor Fe enrichment takes place

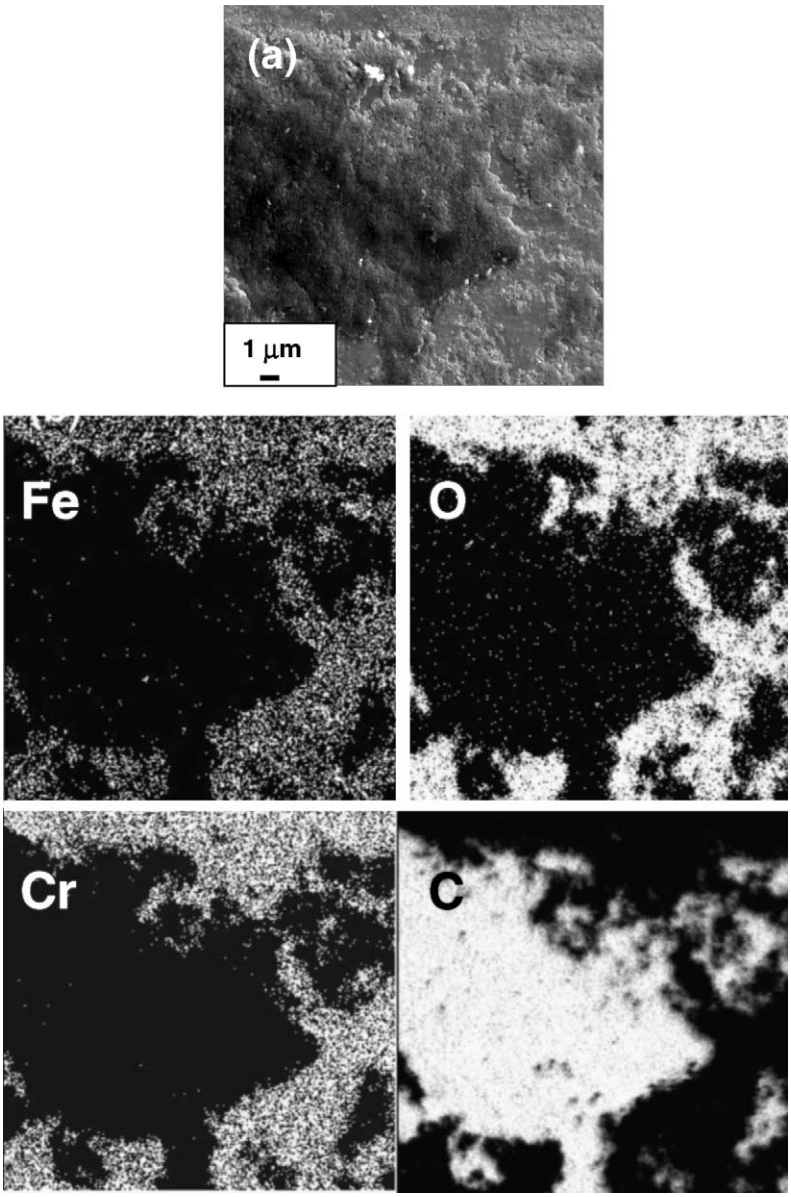

Fig. 3. (a) SEM image of the area where SAM map of Fe, O, C, Cr took place. (b) SAM map of Fe, O, C, Cr on the area shown in the SEM image of Fig. 3a.

within or near the surface. This is in contrast to claims that Ni enrichment takes place for all Ni-Fe alloys leading to selective Fe corrosion [31].

Nonetheless, for the G + EP-surface metal dusting occurs rather severely. The dark shaded area in Fig. 3a contains C as it is shown by the SAM maps in Fig. 3b (maps of Fe, Cr, O, and C). The SAM maps have been taken with an electron beam spot size of 15 nm, and show a lateral resolution ∼40 nm. Backscattered electrons limit SAM map resolution to larger length scales. In the area covered by C, Fe or Cr-oxide are absent indicating strongly a carburization process within the areas of attack. The C attack also occurs along grain boundaries as shown by the dotted lines in Fig. 3a.

At the position of the lower arrow (spot 1) in Fig. 4a, depth profile analysis shows the presence of a thin external C layer (a few nm thick), which is likely due to surface hydrocarbons. The Cr-oxide extends up to a depth ∼300 nm. After this point area 1 starts where the Cr concentration decreases together with the O content up to a depth ∼600 nm exhibiting a minimum. Meanwhile the Fe and Ni contents increase and reach a maximum for Ni at ∼750 nm, which is the point where any O signal vanishes. In the area 2, Ni also decreases with decreasing O content, and this decrement continues towards area 3, while the C increases from area 2 towards area 3. After area 3, Fe, Ni, Cr and C reach constant bulk concentrations. The Cr concentration curve shows an overall depletion width of ∼700 nm (width of areas 1 → 3).

Notably, C was not present within the bulk of the unexposed samples, while it is present within the matrix of the exposed to metal dusting of the G + EP sample surface. Although the Cr-oxide inhibits metal dusting, it cannot prevent C diffusion towards the bulk of the sample. Furthermore, at the location of the second arrow within the dark area, depth profile

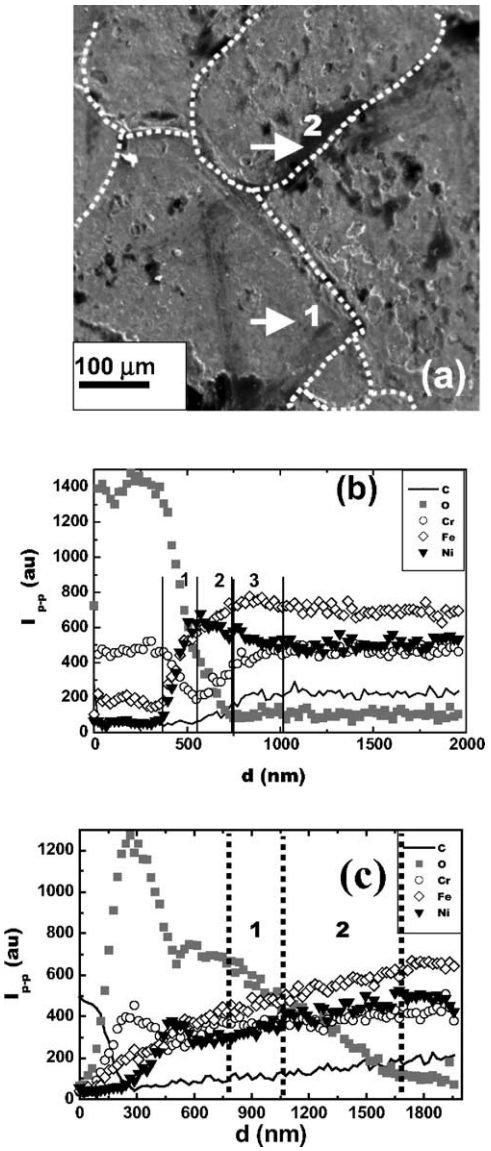

Fig. 4. (a) SEM image of metal dusted ground and electropolished sample surface with the arrows indicating the positions where depth profile was performed with electron beam size 20 μm: (b) Spot 1 in Fig. 3a, and (c) spot 2 in Fig. 3a. The dotted lines in (a) indicate grain boundaries on the sample surface.

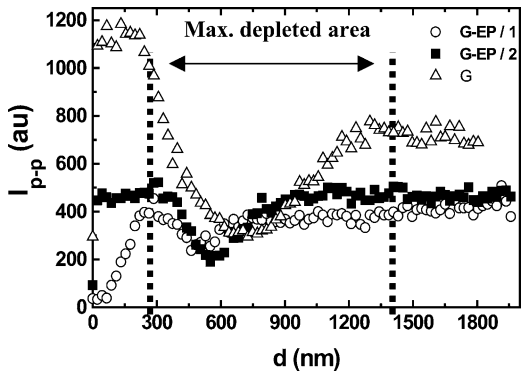

Fig. 5. Peak-to-peak AES signal of Cr for the ground sample of Fig. 2, and for the ground and electropolished surfaces at spots 1 and 2 indicated by arrows (also shown in Figs. 4b and c).

analysis shows a thick C layer outside the sample surface that extends up to a depth ∼250 nm (Fig. 4c). This layer is removed at the point where the Cr peak is maximum. The C peak again increases (linearly with increasing depth $d > 250$ nm), but in contrast to Fig. 4b it extends over a larger depth beyond the point where the oxidation is present (up to a depth ∼1800 nm). In this case no significant Cr-oxide is formed which is seen by the absence of the 'plateau' area for Cr.

For comparison, we show the development of the Cr intensity for all the three cases together in Fig. 5. Clearly, any Cr oxidation occurs up to a depth of 300 nm from the sample surface, while the Cr depleted area is maximum for the G-sample, which is strongly protected against carburization and subsequent metal dusting. From the previous results it is clear that the G + EP surfaces are more subjective to metal dusting than the rougher G-surface. Therefore, the resistance to metal dusting is strongly correlated with the surface finish. Increasing the number of fast diffusion paths for O assists in the nucleation and growth of a protective metal oxide [1–10]. Indeed, if rapid formation of a surface oxide is aided by a suitable surface working technique, protection against internal C attack can be ensured (Fig. 6).

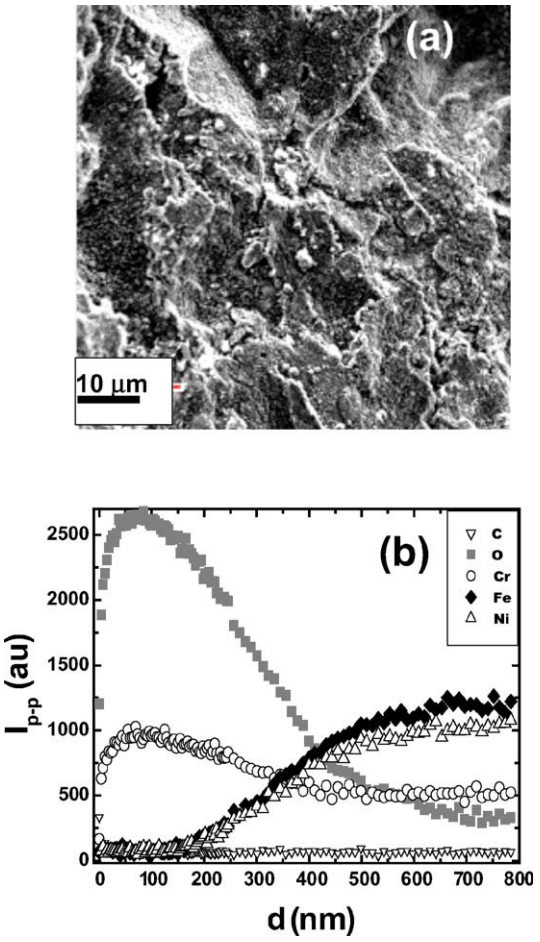

Fig. 6. (a) SEM image of exposed to metal dusting conditions of a sandblasted sample surface. (b) Depth profile analysis with electron beam size 20 μm.

Finally, for the sake of comparison an example of sandblasted surfaces of the same alloy is shown, which there are rough on lateral length scales of tens of microns. Also in this case we detect a behavior similar to that of the G-sample in Fig. 2 where Cr-oxide is formed and any metal dusting process is rather interrupted without any C accumulation within the metal matrix. Therefore, rougher surface area does not necessarily means higher susceptibility to carbonization and metal dusting processes. Depending on the roughening process it is likely that diffusion paths for C within the metal matrix are becoming blocked yielding therefore a higher protection against internal carburization by the additional presence of Cr-oxide.

4. Conclusions

In conclusion, we investigated metal dusting in Fe–Ni–Cr alloys performing scanning Auger/Electron microscopy. It is shown that the formation of surface Cr-oxide, and the surface finish condition can strongly influence and interrupt metal dusting. Depending on the surface roughening process, it is likely that diffusion paths for C within the metal matrix are blocked, yielding therefore better protection against internal carbunization by the additional presence of Cr-oxide. Nonetheless, the accumulation of C within the metal matrix was not always prevented by the Cr-oxide layer. Indeed, it was found that the formation of the Cr-oxide was accompanied by a depleted Cr layer next to the oxide layer with a depth of several hundreds of nanometers. However, the depleted Cr layer was significantly wider if the C diffusion within the metal matrix was blocked by the Cr-oxide layer. At any rate, within the depleted from Cr layer or even closer to the surface neither Ni nor Fe preferential enrichment was

observed, excluding therefore any special influence on metal dusting phenomena.

Acknowledgements

The authors would like to thank their former colleague A. Folkertsma from TNO (Netherlands Organization for Applied Scientific Research) for providing the samples for the AES studies.

References

[1] H.J. Grabke, Carburization–A High Temperature Corrosion Phenomenon, Materials Technology Institute, St. Louis, 1998.
[2] H.J. Grabke, U. Gravenhorst, W. Steinkusch, Werkst. u. Korr. 27 (1976) 91.
[3] A. Schnaas, H.J. Grabke, Oxid. Met. 12 (1978) 387.
[4] H.J. Grabke, A. Schnaas, in: Proceedings of the Petten Institute Conference on Alloy 800 Petten March 1978 Niederlande, North Holland Publishing Company, Amsterdam, 1978, pp. 195–211.
[5] A. Schnaas, H.J. Grabke, Werkst. u. Korr. 29 (1978) 635.
[6] H.J. Grabke, R. Möller, A. Schnaas, Werkst. u. Korr. 30 (1979) 794.
[7] W. Steinkusch, Werkst. u. Korr. 30 (1979) 837.
[8] J.M. Harrison, J.F. Norton, R.T. Derricott, J.B. Marriott, Werkst. u. Korr. 30 (1979) 785.
[9] H.J. Grabke, I. Wolf, Mater. Sci. Eng. 87 (1987) 23.
[10] A. Rahmel, H.J. Grabke, W. Steinkusch, Mater. Corr. 49 (1998) 221.
[11] J.C. Nava Paz, H.J. Grabke, Oxid. Met. 39 (1993) 437.
[12] H.J. Grabke, R. Krajak, J.C. Nava Paz, Corr. Sci. 35 (1993) 1141.
[13] H.J. Grabke, R. Krajak, E.M. Müller-Lorenz, Werkst. u. Korr. 44 (1993) 89.
[14] H.J. Grabke, C.B. Bracho-Troconis, E.M. Müller-Lorenz, Werkst. u. Korr. 45 (1994) 215.
[15] H.J. Grabke, Corros. NACE 51 (1995) 711.
[16] H.J. Grabke, E.M. Müller-Lorenz, Steel Res. 66 (1995) 252.
[17] H.J. Grabke, R. Krajak, E.M. Müller-Lorenz, Strauss, S. Werkst. u. Korr. 47 (1996) 495.
[18] J. Klöwer, H.J. Grabke, E.M. Müller-Lorenz, Mater. Perform (NACE) 37 (1998) 58.
[19] H.J. Grabke, Mater. Corr. 49 (1998) 303.
[20] H.J. Grabke, E.M. Müller-Lorenz, Mater. Corr. 49 (1998) 317.
[21] E. Pippel, J. Woltersdorf, S. Strauss, H.J. Grabke, Steel Res. 66 (1995) 217.
[22] R. Schneider, E. Pippel, J. Woltersdorf, S. Strauss, H.J. Grabke, Steel Res. 68 (1997) 326.
[23] E. Pippel, J. Woltersdorf, R. Schneider, Mater. Corr. 49 (1998) 309.
[24] C.M. Chun, T.A. Ramanarayanan, J.D. Mumford, Mater. Corr. 50 (1999) 634.
[25] A. Schneider, H. Viefhaus, G. Inden, H.J. Grabke, E.M. Müller-Lorenz, Mater. Corr. 49 (1998) 330.
[26] A. Schneider, H. Viefhaus, G. Inden, H.J. Grabke, Werkstoffwoche ’98 München, Symposium 7 Band III, Wiley, p. 399 (Chapter V).
[27] H.J. Grabke, Mater. High Temp. 17 (2000) 483;
H.J. Grabke, Mater. Technol. 36 (2002) 6.
[28] S. Strauss, H.J. Grabke, Mater. Corr. 49 (1998) 321.
[29] D.T.L. van Agterveld, G. Palasantzas, J.Th.M. De Hosson, Appl. Surf. Sci. 152 (1999) 250;
D.T.L. van Agterveld, G. Palasantzas, J.Th.M. De Hosson, Act. Mater. 48 (2000) 1995.
[30] M.L. Holland, H.J. De Bruyn, Int J. Pres. Ves. Piping 66 (1996) 125.
[31] E. Rippel, J. Woltersdorf, H.J. Grabke, Metal dusting of iron-nickel alloys: Development of composition-dependent microstructures (see also the site: http://www2.umist.ac.uk/corrosion/conferencefinal/High_Temperature_Corrosion/Abstracts/H035.HTM).